A Comparative Study of Heaterless Hollow Cathode: 2D PIC Modeling vs. Experiment

IEPC-2013-380

Presented at the 33rd International Electric Propulsion Conference,
The George Washington University • Washington, D.C. • USA
October 6 – 10, 2013

V. Vekselman[1]
Department of Material Science and Engineering, Clemson University, Clemson, SC, 29634, USA

D. Levko[2]
LAPLACE (Laboratoire Plasma et Conversion d'Energie), Universite de Toulouse, UPS, INPT Toulouse, 118 route de Narbonne, F-31062 Toulouse cedex 9, 31062, France

Ya. E. Krasik[3]
Department of Physics, Technion, Haifa, 32000, Israel

and

I. Haber[4]
University of Maryland, College Park, Maryland 20742-3511, USA

Abstract: One of the most exciting advances in plasma propulsion area has been the development of electron source based on thermionic hollow cathode DC discharge. Unfortunately, most thermionic hollow cathodes are still incorporated with an external heater for an ignition procedure that increases power consumption, ignition time, design complexity and decreases cathode reliability and possible applications (e.g., in microsatellite propulsion sector). As a result, a heaterless design of thermionic hollow cathodes has been proposed by several research groups. In this paper we describe results of a heaterless orificed hollow cathode experimental study and results of a self-consistent two-dimensional (2D) Particle-in-Cell (PIC) Monte Carlo collision (MCC) modeling developed in WARP environment, which we use to compare the cathode operation in DC mode. The experimental study was done using double Langmuir probe, retarding energy analyzer, biased collimated Faraday cup and spatial resolved optical spectroscopy. The modeling accounts for thermionic electron emission including the Schottky effect, secondary electron emission due to bombardment by the plasma ions, different collision processes and non-uniform *Xe* gas density distribution in the cathode-anode gap. As a result, plasma parameters – density, energy distribution function and potential distribution reflect the experimentally obtained plasma parameters fairly well. Correlation of simulation and experimental results for

[1] Postdoctoral Fellow, Department of Material Science and Engineering, vveksel@clemson.edu.
[2] Postdoctoral Fellow, Laboratoire Plasma et Conversion d'Energie, dima.levko@gmail.com.
[3] Professor, Department of Physics, fnkrasik@physics.technion.ac.il.
[4] Professor, University of Maryland.

particular cathode geometry and operational parameters allows us to conclude that the description of physical phenomena accompanying the heaterless hollow cathode operation in the simulation code is correct. We expect that developed self-consistent 2D PIC MCC code will make it significantly easier for researchers to model the hollow cathode operation and predict its operational parameters for different geometries, *Xe* flow rates and applied voltages with high accuracy.

Nomenclature

CFC	=	collimated Faraday cup
dt_{in}	=	time between ion-neutral collision
dt_{en}	=	time between electron-neutral collision
E	=	electric field
HC	=	hollow cathode
HTHC	=	heaterless thermionic hollow cathode
P	=	gas pressure
PIC	=	particle-in-cell
REA	=	retarding energy analyzer
THC	=	thermionic hollow cathode
T_g	=	Xe gas temperature
SEE	=	secondary electron emission

I. Introduction

Conventional heater based thermionic hollow cathode (THC) is the most popular source of choice for high performance plasma propulsion systems. While it mostly serves as a source of electrons[1-3], there are implementations of THC as an all-in-one plasma thruster[4]. Such popularity of THCs is based on their ability to generate higher electron current density at lower magnitude of applied voltage as compared with cathodes based on planar cathode geometry. The phenomenon responsible for this cathode performance enhancement is called hollow cathode (HC) effect. In general, the HC effect is an additive effect originated from various mechanisms of electron generation, e.g., a photon induced secondary emission, electron oscillations within the plasma volume due to formation of cathode sheath, ionization in the cathode fall, and an ion induced secondary electron emission. Contribution of each electron generation mechanism depends on the cathode geometry, materials and environmental conditions.

Thermionic (hot) hollow cathode utilizes an insert – special refractory material having low work function – for thermionic electron emission given by Richardson-Dushman equation.[5] Formation of the cathode sheath leads to additional enhancement of the extracted electron current density due to the Schottky effect.[6] These electrons accelerated within the cathode sheath oscillate between cathode falls regions effectively ionizing the residual gas and forming dense plasma. As a result, at certain conditions an ion flux from the plasma boundary toward the insert is able to provide sufficient energy to the insert to operate the cathode in self-heating mode. Thus, an external heater is required only for the cathode ignition procedure. However, due to necessity in external heater the conventional THC has several disadvantages limiting its use in certain applications. Namely, start-up (ignition) procedure takes several minutes at considerable power consumption, heater affects the cathode durability and together with additional power supply increases the total weight of the system. The cathode life time becomes dependent on two major effects: insert material poisoning and heater failure. Possible solution of these drawbacks is development of heater-less thermionic hollow cathode (HTHC). Design of HTHC was proposed and implemented by Schatz, Arkhipov, Sarvey-Verhey and Hamley, Gallimore, Koroteev, and other researchers. However, these HTHCs have not yet being used in space flight demanding further reduction of power consumption, more reliability, more robust design and longer life time.

In this paper we present experimental study and modeling of the heater-less thermionic hollow cathode designed in Kharkiv Aerospace University (KhAI).[7] A reliable operation of this cathode within preferred range of extracted currents dictates certain parameters of Xe flow rate, emitter temperature, cathode-anode voltage, cathode geometry and thermionic properties of emitter (insert).[8] Any change in the extracted current amplitude leads to self-consistent

adjusting of the plasma parameters inside the cathode. Investigation of plasma parameters inside the cathode, especially in the vicinity of thermionic emitter, is a formidable challenge for each researcher due to tiny space, invisibility, inaccessibility and huge plasma perturbation induced by any probes. One indication of validity of the approach in realization of the heaterless hollow cathode design is a self-consistent modeling of the cathode operation.

II. Models, Methods and Diagnostics

The two-dimensional Cartesian module of the open-source WARP PIC code[9] was employed for modeling of heater-less thermionic hollow cathode shown in Fig. 1. A multi-grid Poisson solver encapsulated in WARP code was applied to obtain the self-consistent electrostatic fields. The model employed two space and two velocity (2D-2V) components.

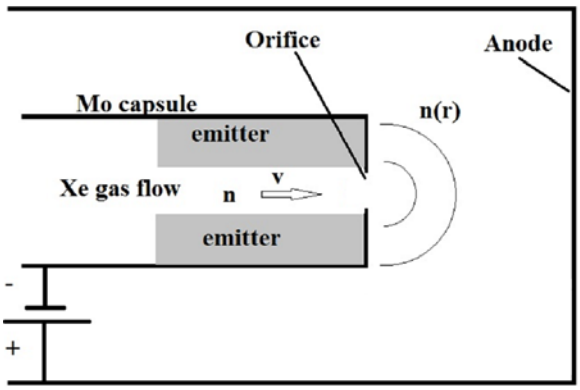

Figure 1. Geometry of HTHC used in simulation.

This model describes thermionic electron emission from the insert (emitter) including the Schottky effect, non-uniform Xe gas density distribution in the cathode-anode gap, and secondary electron emission due to cathode bombardment by the plasma ions. However, self-consisted solution for energy fluxes toward the emitter and cathode walls is not yet implemented therefore the emitter temperature is fixed. Neutrals are considered as a background with a uniform density distribution inside the HTHC and non-uniform distribution outside the HTHC. As a result, parameters of the HTHC can be obtained as a function of gas pressure, orifice size, and applied potentials. In current simulation the gas pressure is 150 Torr, emitter and gas temperature 1500 K. More information about the model can be found in Ref 10.

One time step of the simulation code is illustrated in the Fig. 2 which shows the flowchart.

A. Electron emission

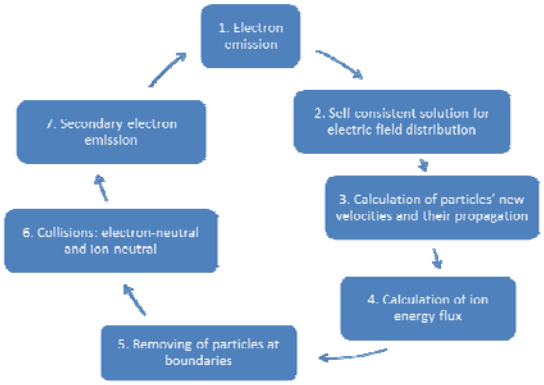

Figure 2. Flowchart for PIC scheme.

Thermionic electron current density is calculated as

$$J(x) = DT^2 \exp\left(\frac{-e\varphi_0}{kT}\right) \cdot \exp\left(\frac{e}{kT}\sqrt{\frac{eE_C(x)}{4\pi\varepsilon_0}}\right) \qquad (1)$$

Here, $D = 1.2\times10^6$ A·m^{-2}K^{-2} is a constant, e is an electric charge, $\varphi_0 = 1.5$ eV is work function of the emitter, T is temperature of the emitter, $E_C(x)$ is electric field at the cathode surface; the second exponent is responsible for Schottky effect. The value of the electric field $E_C(x)$ is calculated by solving the Poisson equation.

B. Collisions

Collisions between particles in plasma discharge are responsible for numerous phenomena and have to be correctly implemented in PIC simulation. We consider electron-neutral (*e-n*) and ion-neutral (*i-n*) collisions for investigated cathode. Coulomb collisions (electron-ion) can be neglected as was shown in Ref 10.

The *e-n* collision model for xenon gas discharge in HTHC includes:

- $e + Xe \rightarrow e + Xe$ - elastic scattering
- $e + Xe \rightarrow e + Xe^*$ - excitation (only the first excitation energy level of Xe is considered)
- $e + Xe \rightleftarrows e + Xe^+ + e$ - ionization and recombination

The null-collision concept is implemented for *e-n* collision model. For a detail description of the null-collision modeling please refer to Ref 11.

The *i-n* collision model includes:

- $Xe^+ + Xe \rightarrow Xe^+ + Xe$ - elastic scattering

- $Xe^+ + Xe \rightarrow Xe + Xe^+$ - charge exchange

Due to significantly smaller mobility of Xe as compared to electrons, the time step dt_{in} was introduced for *i-n* collisions, $dt_{in} \gg dt_{en}$, where dt_{en} is a time step between *e-n* collisions.

The cross section of charge-exchange collision is calculated as[12]

$$\sigma_{CE} = (k_1 \cdot \ln|\upsilon_{ion} - \upsilon_n| + k_2)^2 \times 10^{-20}\ [m^2] \quad (2)$$

Here $k_1 = -0.8821$ and $k_2 = 15.1262$ are the constants, υ_{ion} is the ion velocity, and υ_n is the neutral velocity chosen randomly from the Maxwellian distribution with temperature T. The elastic scattering cross section is defined as[13]

$$\sigma_{EL} = 6.42 \times 10^{-16} / |\upsilon_{ion} - \upsilon_n|\ [m^2] \quad (3)$$

and the probability for each ion to experience collision with a neutral as

$$P = 1 - \exp(|\upsilon_{ion} - \upsilon_n| dt_{ion} / \lambda) \quad (4)$$

where dt_{ion} is the time step used for ion-neutral collision, and λ is the ion mean free path in the neutral gas.

For a detailed description of the model used for calculation of ion-neutral collisions, see Ref. 14.

C. Secondary electron emission

Secondary electron emission (SEE) coefficient is defined as:[15]

$$k_{\text{sec}} = 0.01 + 3 \times 10^{-5} \cdot \varepsilon_{ion}^{1.455}. \quad (2)$$

Here ε_{ion} is the energy of the incident ion.

D. Experimental diagnostics

Experimental study of the HTHC was carried out using electrical probes and non-disturbing visible spectroscopy technique.[8] The setup is presented in Fig. 3.

Small dimensions of the HTHC considerably complicate investigation of plasma parameters upstream of the cathode orifice plate having an output hole diameter of 100-200 μm. Whereas few sophisticated diagnostics were proposed their successful implementation were reported for larger cathode only. Therefore, only plasma in the orifice-anode region was studied using double Langmuir probe, retarding energy analyzer (REA), collimated Faraday cup (CFC) and non-disturbing spectroscopic technique.

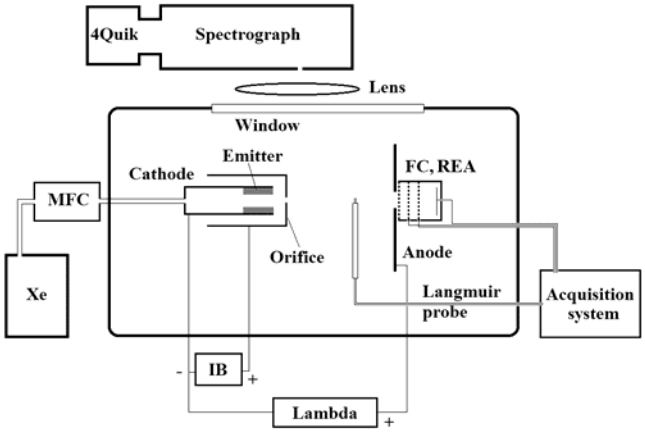

Figure 3. Sketch of experimental setup.

III. Results and Discussions

2D Potential distribution in simulation area in steady state mode of the HTHC operation is presented in Fig. 3.

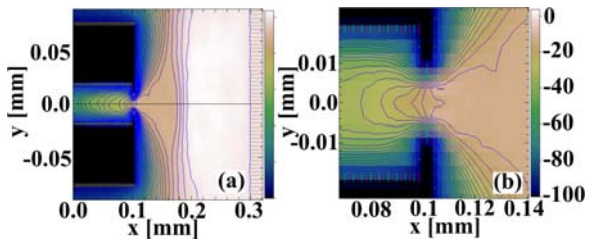

Figure 4 (left). 2D potential distribution in (a) simulation area and (b) zoomed area in the vicinity of the orifice plate; steady state operation of the HTHC.

In order to decrease the computation time in the simulations, all the dimensions were decreased by 10 times. The value of the electric field *E* and ratio *E*/*P*, which

determine the type of electron collisions, were kept as in the actual geometry.
This confirms the formation of region inside the hollow cathode with positive potential relative to the cathode wall. The radial distribution of potential taken at the middle of the hollow cathode (red line), in the vicinity of the orifice plate (blue line) and in the middle of orifice (green line) is shown in Fig. 5(a). Thus plasma ions originated at the cathode axes may acquire as much as 80 eV energy on their way to the cathode wall. Axial potential distribution is presented in Fig. 5(b). The flat part of the potential profile indicates on formation of very conductive plasma in the orifice that expands toward the anode forming the cathode plume.

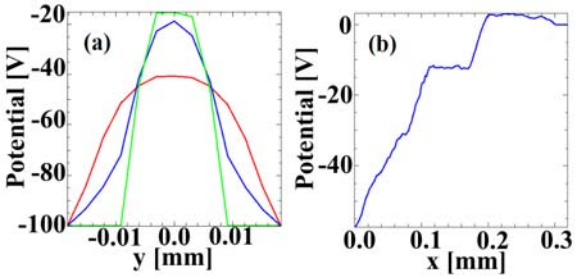

Figure 5. (a) Radial potential distribution in the middle of the hollow cathode (red), in the vicinity of the orifice plate (blue) and in the middle of orifice (green); (b) axial potential distribution.

The plasma electron and ion density distribution is presented in Fig. 6. It was obtained that the largest plasma density is in the vicinity of the orifice output hole. The regions with dilute plasma are in the vicinity of the cathode walls, between the cathode plume and the slightly positively charged plasma and in the vicinity of the anode. Similar picture was obtained by visual observation of the cathode operation and was confirmed by spectroscopy (see Fig. 7).

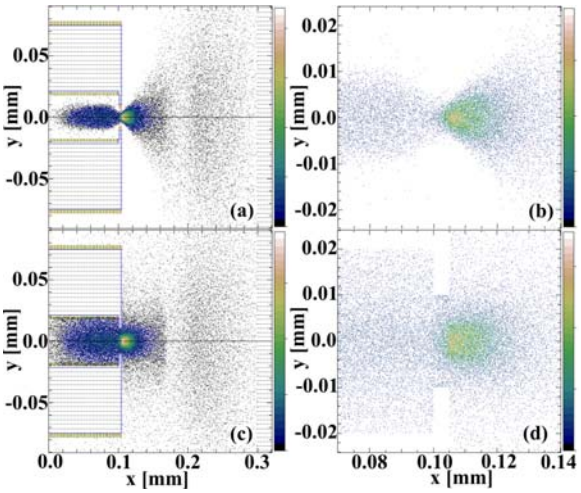

Figure 6 (above). Density distribution of electrons (a,b) and ions (c,d) in steady state mode of the HTHC operation.

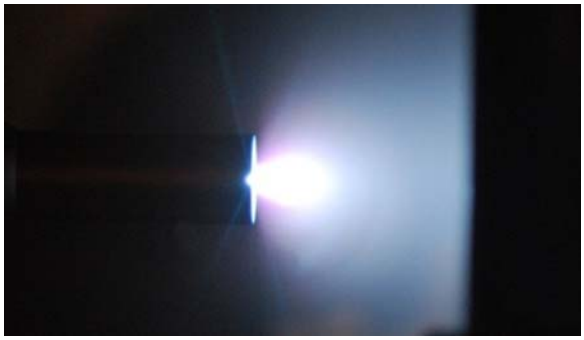

Figure 7 (right). Visible observation of the cathode plasma plume during the HTHC operation.

Figure 8 (bottom). Density profile of the plasma plume obtained by spectroscopy study.

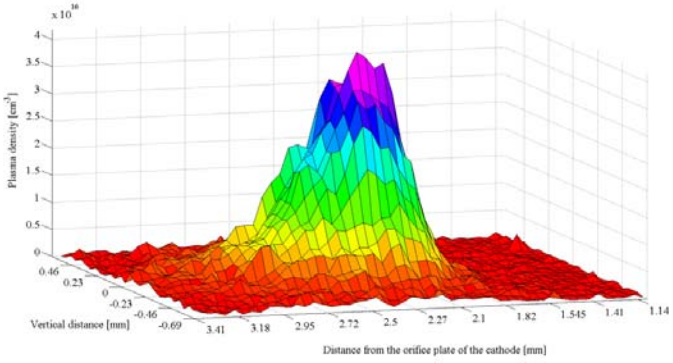

A spectroscopic study of the cathode plasma plume reveal the maximum plasma density of $4 \cdot 10^{16}$ cm^{-3}, see Fig. 8. Measurements of the plasma parameters by double Langmuir probe between plasma plume and the anode show that plasma density in this region is 10^{10}-10^{11} cm^{-3} and plasma electron temperature is around 2 eV. These results are in a good agreement with simulation results. The transverse (along the Y-axis) density distribution of plasma particles at different positions along X – axis (see Fig. 9) shows that the largest plasma density is realized at y = 0 (cathode axis). A quasi-constant density of the plasma electrons and ions occurs only in the narrow region with a width of a few microns inside the orifice and ~200 μm inside the HC; further, the density of plasma particles decreases rather

rapidly with the distance from the Y-axis, showing formation of plasma sheaths in the vicinity of the HC and orifice walls.

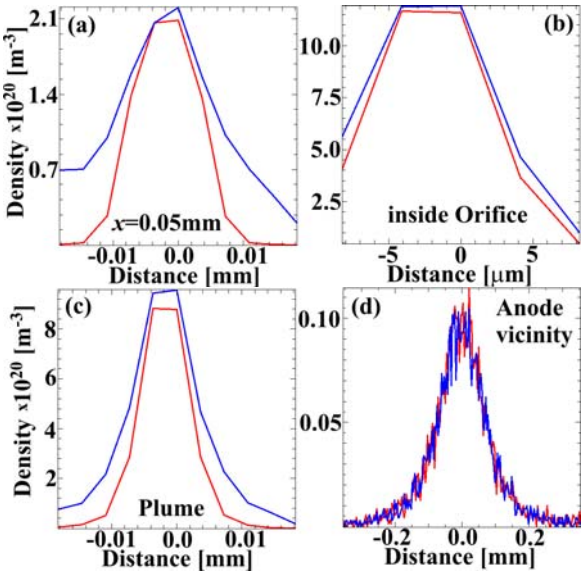

Figure 9. Transversal profile of electron (red line) and ion (blue line) density at different positions along cathode axis (x-axis).

The electron velocity phase space [see, Fig. 10(a,b)] and electron energy distribution function [see Fig. 11(a,b)] show an electron beam, which is generated in the double sheath formed between the cathode plasma plume and the slightly positive anode plasma. One can see that electrons acquire energies up to 20 eV, which agrees with the energy spectrum of electrons measured behind the anode by retarding energy analyzer and collimated Faraday cup. These energetic electrons propagate toward the anode almost without collisions, because the mean free path of these electrons in neutrals ($n_n \leq 5\times10^{23}$m^{-3}) and plasma ($n_{pl} \leq 10^{19}$m^{-3}) is significantly larger than the propagation distance. In the cathode plasma plume and the slightly-positively-charged anode plasma, the main part of electrons can be characterized by a Maxwellian velocity distribution with mean energy of ~2 eV [see Fig. 11(b)]. However, one can find rather energetic electrons at the tail of this velocity distribution.

Inside the HC plasma, the electron velocity distribution is rather broad because of oscillating electrons and it can be characterized by a mean energy of electrons of ~5 eV [see Fig. 10(a) and 11(a)].

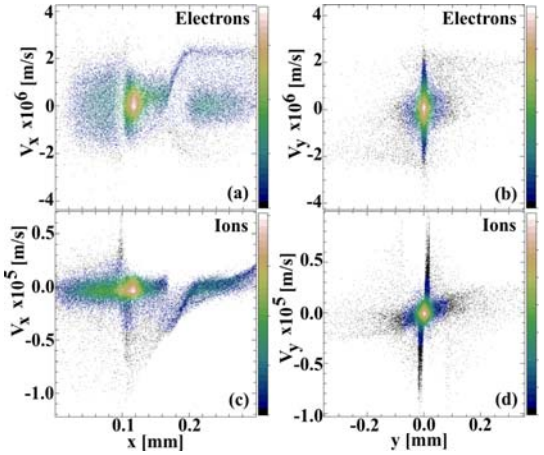

Figure 10. Electron (a,b) and ion (c,d) phase space in the steady state of the HC operation.

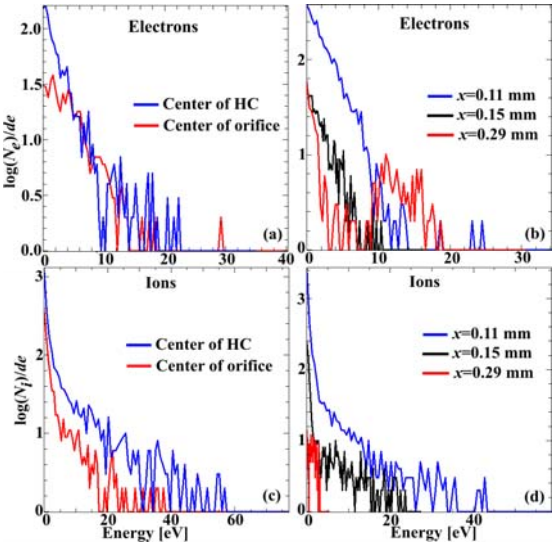

Figure 11. Electron (a,b) and ion (c,d) energy distribution functions in the steady state of the HC operation obtained at different axial planes.

IV. Conclusion

A self-consistent 2D PIC Monte Carlo collision model was developed and used for the numerical simulation of the operation of the heaterless thermionic hollow cathode. Initial parameters used in simulation precisely reflect the geometry of the HTHC, estimated Xe gas pressure, and measured applied voltage. The model includes thermionic electron emission, SEE, electron-ion recombination and different electron-neutral collision processes, and non-uniform Xe gas density in the cathode-anode gap. The numerical simulations allow one to determine plasma particle density and energy at different locations of the HTHC, potential distribution and energy flux toward the HC and

orifice walls. The simulations showed the formation inside the HC of a sheath between the plasma acquiring positive potential and the emitter, with potential differences up to several tens of Volts. In addition, a double sheath formation between the cathode plasma plume and the anode plasma was obtained in these simulations. Electron acceleration in this double sheath leads to generation of an energetic electron flux toward the anode. Significant deviation of the electron energy distribution from the Maxwellian energy distribution was obtained. In addition, it was shown that the energy of ions accelerating inside the cathode sheath can reach tens of eV, which could lead to fast erosion of the emitter and orifice. Finally, the denser plasma was obtained in the vicinity of the output of the orifice. All simulation results are inagreement with experimental study of the HTHC operation in diode mode. We believe that the developed 2D PIC Monte-Carlo collision code can predict operational characteristics of various cathodes with high accuracy.

References

[1]Jahn, R., and Choueiri, E., *Electric Propulsion in Encyclopedia of Physical Science and Technology*, 3rd ed., Academic Press, San Diego, 2002, v.5, pp. 125-141.

[2]Finke, R., *Electric Propulsion and Its Applications to Space Missions*, Progress in Astronautics and Aeronautics, v. 79, AIAA, 1981.

[3]Goebel, D., Katz, I., *Fundamentals of Electric Propulsion*, John Wiley & Sons, 2008.

[4]Grubisic, A.N. and Gabriel, S.B., "Preliminary thrust characterization of a T5 hollow cathode" in 43rd AIAA/ASME/SAE/ASEE Joint Propulsion Conference & Exhibit, Cincinnati, Ohio, 08 - 11 Jul 2007, USA.

[5]Dushman, S., "Thermionic emission", *Rev. Mod. Phys*. Vol. 2, 381–476 (1930).

[6]Fowler, R.H., Nordheim, L.,"Electron Emission in Intense Electric Fields", Proceedings of the Royal Society A, 119 (781): 173–181, 1928.

[7]Koshelev, N., and Loyan, A., "Investigation of Hollow Cathode for Low Power Hall Effect Thruster", 30th Int. Electric Propulsion Conference, IEPC 2007-103, Florence, Italy, 16-20 Sept. 2007.

[8]Vekselman, V., Krasik, Ya., E., Gleizer, S., Gurovich, V., Tz., Warshavsky, A., and Rabinovich, L., "Characterization of a Heaterless Hollow Cathode", *J. Propulsion and Power*, Vol. 29, 475, 2013.

[9]Grote, D., P., Friedman, A., Vay, J., L., Haber, I., "The WARP Code: Modeling High Intensity Ion Beams", AIP Conf. Proc. 749, pp. 55-58, 2005.

[10]Levko, D., Krasik, Ya., E., Vekselman,V., and Haber, I., "Two-dimensional model of orificed micro-hollow cathode discharge for space application" *Phys. Plasmas* Vol. 20, 083512, 2013.

[11]Vahedi, V., Surendra, M., "A Monte Carlo collision model for the particle-in-cell method: applications to argon and oxygen discharges" *Comp. Phys. Comm*. Vol. 87, 179, 1995.

[12]Rapp, D., and Francis, W., E., "Charge Exchange between Gaseous Ions and Atoms", *J. Chem. Phys*. Vol. 37, 2631, 1962.

[13]Dalgarno, A., McDowell, M., R., C., and Williams, A., "The Mobilities of Ions in Unlike Gases", Phil. Trans. R. Soc. Lond. A, Vol. 250, 411, 1958.

[14]Nanbu, K., "Simple Method to Determine Collisional Event in Monte Carlo Simulation of Electron-Molecule Collision", Jpn. J. Appl. Phys., Vol. 33, pp. 4752-4753, 1994.

[15]Yang, S., S., Lee, S., M., Iza, F., and Lee, J., K., "Secondary electron emission coefficients in plasma display panels as determined by particle and fluid simulations", *J. Phys. D: Appl. Phys*., Vol.39, 2775, 2006.